PHYSICAL REVIEW D **82,** 026006 (2010)

Boost invariant flow, black hole formation, and far-from-equilibrium dynamics in $\mathcal{N} = 4$ supersymmetric Yang-Mills theory

Paul M. Chesler* and Laurence G. Yaffe†

Department of Physics, University of Washington, Seattle, Washington 98195, USA

(Received 23 April 2010; published 19 July 2010)

Using gauge/gravity duality, we study the creation and evolution of boost-invariant anisotropic, strongly-coupled $\mathcal{N} = 4$ supersymmetric Yang-Mills plasma. In the dual gravitational description, this corresponds to horizon formation in a geometry driven to be anisotropic by a time-dependent change in boundary conditions.

DOI: 10.1103/PhysRevD.82.026006 PACS numbers: 11.25.Tq

I. INTRODUCTION

The study of nonequilibrium phenomena in QCD and other non-Abelian quantum field theories is a topic of much interest, with applications to heavy-ion collisions, early universe cosmology, and other areas. Much has been learned about near-equilibrium dynamics at weak coupling where a quasiparticle picture is valid [1–5], and there has also been considerable progress understanding certain theories at very strong coupling [6–9], thanks to the development of gauge/gravity duality [10–12]. But very little progress has been made in regimes where a theory is both strongly coupled and far from equilibrium.

Heavy-ion collisions at the Relativistic Heavy Ion Collider (RHIC) are believed to produce a deconfined, strongly-coupled quark-gluon plasma (QGP) [13,14]. In the initial stages of the collision, during which the QGP is produced, the system is surely far from equilibrium and cannot be described by hydrodynamics. However, modeling based on near-ideal hydrodynamics strongly suggests that a hydrodynamic treatment becomes applicable rather quickly, perhaps on times $\lesssim 1$ fm/c after the collision event [15]. Understanding the dynamics responsible for such a rapid approach to local equilibrium from a far-from-equilibrium initial state is a challenge.

Colliding nuclei at sufficiently high energy is the only experimentally accessible approach for creating quark-gluon plasma. However, analyzing the dynamics—from the creation of the initial highly nonequilibrium state, through partial equilibration, hydrodynamic evolution, hadronization, and eventual freeze out—via a first principles calculation in QCD is not currently possible. Nevertheless, aspects of this process involving strongly-coupled dynamics can be studied in a controlled setting in a class of theories which describe non-Abelian plasmas similar to the QGP, and which possess dual gravitational descriptions. The best known example is $\mathcal{N} = 4$ supersymmetric Yang-Mills (SYM) theory [10]. In this theory, one can study the collision of shock waves using gauge/gravity duality [16–19]. The shock waves have a very small thickness along the collision axis and can be localized in the transverse directions [20]. Therefore, qualitatively at least, they resemble the Lorentz-contracted relativistic nuclei in a heavy-ion collision.

In the dual gravitational description, collisions of shock waves in SYM turn into a problem of colliding gravitational shock waves in five dimensions. The resulting 5D numerical relativity problem is still quite challenging, but may be feasible using techniques which are adapted from current work in 4D numerical relativity. One purpose of this paper is to begin exploring some of the needed adaptations, albeit in a setting which is simpler than colliding shock waves.

The immediate goal of this paper is to study how quickly a far-from-equilibrium strongly-coupled non-Abelian plasma relaxes to a regime in which a hydrodynamic description is accurate. The answer to this question will necessarily have some sensitivity to how the initial state is created. A conceptually simple way to prepare nonequilibrium states is to start in the ground state, and then to turn on time-dependent background fields coupled to operators of interest. After the background fields are turned off, one can then watch the subsequent evolution of the system. Since a hydrodynamic description requires that the stress tensor (in the local fluid rest frame) be nearly isotropic [3], particularly interesting initial states are those in which the initial stress tensor is driven to be highly anisotropic. A natural way to do this is to make the spatial geometry in which the field theory lives be time dependent and anisotropic [21,22].

At weak coupling, the addition of energy to the ground state by a time-dependent gravitational field can be understood in terms of particle production. A time-dependent spacetime geometry will create quanta [23], and if the time dependence of the deformation in the geometry is anisotropic, then the momentum distribution of created quanta will be anisotropic as well. After the geometry ceases to evolve, quanta will continue to collide and interact and eventually (on a time scale which at weak coupling diverges like $1/\lambda^2$, with λ the 't Hooft coupling) the system

*pchesler@u.washington.edu
†yaffe@phys.washington.edu

may approach a state in approximate local thermal equilibrium.

This quasiparticle picture breaks down as the strength of the coupling increases, and one must understand the process of plasma production and relaxation using a different physical description. For large N_c SYM, gauge/gravity duality provides an alternative picture involving black hole formation in five dimensions. As we discuss in Sec. II, the gravitational dual will involve a 5D curved spacetime with a 4D boundary which has a time-dependent geometry. The boundary geometry corresponds to the spacetime geometry of the SYM field theory. A time-dependent deformation in the 4D boundary geometry will produce gravitational radiation which propagates into the fifth dimension. This radiation will necessarily produce a black hole [21]. It is natural that the gravitational description of plasma formation and relaxation involves horizon formation, since at late times the system will be in a near-equilibrium state with nonzero entropy.

The presence of a black hole acts as an absorber of gravitational radiation and therefore, after the production of gravitational radiation on the boundary ceases, the 5D geometry will relax onto a smooth and slowly varying form. This relaxation is dual to the relaxation of nonhydrodynamic degrees of freedom in the quantum field theory [9]. Therefore, by studying the evolution of the 5D black hole geometry, one can gain insight into the creation and relaxation SYM plasma.

For simplicity, in this paper we limit attention to 4D geometries which have two-dimensional spatial homogeneity and $O(2)$ rotation invariance in the $\boldsymbol{x}_\perp \equiv \{x^1, x^2\}$ directions, and which are invariant under boosts in the $x_\parallel \equiv x^3$ direction. As we discuss in Sec. II, this reduces the gravitational dynamics to a system of two-dimensional partial differential equations, which we solve numerically. Besides making the gravitational calculation simpler, these assumptions serve an additional purpose. With these symmetries, the late-time asymptotics of the 5D geometry (and the corresponding asymptotics of the stress tensor) are known analytically [24–26]. We will therefore be able to compare directly our numerical results, valid at all times, to the known late-time asymptotics.

Boost invariance implies that the natural coordinates to use are proper time τ and rapidity y (with $x^0 \equiv \tau \cosh y$ and $x_\parallel \equiv \tau \sinh y$). In these coordinates, the metric of 4D Minkowski space (in the interior of the $\tau = 0$ cone) is $ds^2 = -d\tau^2 + d\boldsymbol{x}_\perp^2 + \tau^2 dy^2$. A deformation of the geometry, respecting the above symmetry constraints, induced by a time-dependent shear may be written in the form

$$ds^2 = -d\tau^2 + e^{\gamma(\tau)} d\boldsymbol{x}_\perp^2 + \tau^2 e^{-2\gamma(\tau)} dy^2. \tag{1}$$

The function $\gamma(\tau)$ characterizes the time-dependent shear; neglecting 4D gravity, $\gamma(\tau)$ is a function one is free to choose arbitrarily. For this study, we chose

$$\gamma(\tau) = c\Theta(1 - (\tau - \tau_0)^2/\Delta^2)[1 - (\tau - \tau_0)^2/\Delta^2]^6 \times e^{-1/[1-(\tau-\tau_0)^2/\Delta^2]}, \tag{2}$$

with Θ the unit step function. [Inclusion of the $[1 - (\tau - \tau_0)^2/\Delta^2]^6$ factor makes the first few derivatives of $\gamma(\tau)$ better behaved as $\tau - \tau_0 \to \pm\Delta$.] The function $\gamma(\tau)$ has compact support and is infinitely differentiable; $\gamma(\tau)$ and all its derivatives vanish at the endpoints of the interval (τ_i, τ_f), with $\tau_i \equiv \tau_0 - \Delta$ and $\tau_f \equiv \tau_0 + \Delta$. We choose $\tau_0 \equiv \frac{5}{4}\Delta$ so the geometry is flat at $\tau = 0$.[1] We choose to measure all dimensionful quantities in units where $\Delta = 1$ (so $\tau_i = 1/4$ and $\tau_f = 9/4$).

Figure 1 shows a spacetime diagram schematically depicting several stages in the evolution of the SYM state. Hyperbola inside the forward light cone are constant τ surfaces. Prior to $\tau = \tau_i$, the system is in the ground state. The region of spacetime where the geometry is deformed from flat space is shown as the red region labeled I in Fig. 1. At coordinate time $t = \tau_i$ the geometry of spacetime begins to deform in the vicinity of $x_\parallel = 0$. As time progresses, the deformation splits into two localized regions centered about $x_\parallel \sim \pm t$, which subsequently separate and move in the $\pm x_\parallel$ directions at the speeds asymptotically approaching the speed of light. After the ''pulse'' of spacetime deformation passes, the system will be left in an excited, anisotropic, nonequilibrium state. That is, the deformation in the geometry will have done work on the field theory state. This region, labeled II, is shown in yellow in Fig. 1. It is in this region that we can study the relaxation of a far-from-equilibrium nonequilibrium state. After some amount of proper time τ_*, the system will have relaxed to a point where a hydrodynamic description of the continuing evolution is accurate. This final hydrodynamic regime is shown schematically in green, and labeled III, in Fig. 1. As the late-time hydrodynamic solution to boost-invariant flow is known analytically, we choose to define τ_* precisely as the time beyond which the stress tensor coincides with the hydrodynamic approximation to within 10%.

Our task then is to find τ_* and, in particular, see how it correlates with quantities such as the effective temperature T_* at time τ_*. In the $c \to \infty$ limit, which corresponds to a diverging size of the deformation in the 4D geometry, it is inevitable that τ_* approaches τ_f. This is natural in conformal theories, since relaxation times of nonhydrodynamic degrees of freedom are set by the local energy density, and this diverges when $c \to \infty$. In other words, in the limit

[1]Choosing $\tau_0 \geq \Delta$ is convenient for numerics as our coordinate system becomes singular on the $\tau = 0$ light cone. The particular choice $\tau_0 = \frac{5}{4}\Delta$ was made so that our numerical results (which begin at $\tau = 0$) contain a small interval of unmodified geometry before the deformation turns on. For an interesting discussion of nonequilibrium boost-invariant states near $\tau = 0$ see Ref. [27].

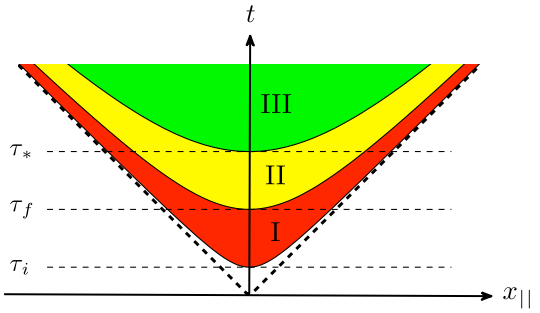

FIG. 1 (color online). A spacetime diagram depicting several stages of the evolution of the field theory state in response to the changing spatial geometry. At proper time $\tau = \tau_i$, the 4D spacetime geometry starts to deform. The region of spacetime where the geometry undergoes time-dependent deformation is shown as the red region, labeled I. After proper time $\tau = \tau_f$, the deformation in 4D spacetime geometry turns off and the field theory state is out of equilibrium. From proper time τ_f to τ_*, shown as the yellow region, labeled II, the system is significantly anisotropic and not yet close to local equilibrium. After time τ_*, shown in green and labeled III, the system is close to local equilibrium and the evolution of the stress tensor is well described by hydrodynamics.

where $1/T_* \ll \Delta$, the system responds adiabatically to the deformation in the geometry and nonhydrodynamic degrees of freedom can remain in equilibrium. A hydrodynamic description (without driving terms) will be accurate the moment the geometry stops changing. Hence, in this limit one learns nothing about the dynamics associated with the relaxation of nonhydrodynamic modes.

More interesting is the case where the effective temperature satisfies $1/T_* \gtrsim \Delta$. This is the regime we will study. Within this regime, the system can be significantly out-of-equilibrium after the 4D geometry becomes flat. When this is the case, we find that the entire process of plasma creation and relaxation to approximate local equilibrium (i.e., to a point where subsequent evolution is accurately described by viscous hydrodynamics) occurs over a time which varies between 1 and 2 times $1/T_*$.

This result is consistent with the findings in our earlier work [21] where we studied isotropization in a homogeneous strongly-coupled $\mathcal{N} = 4$ SYM plasma. In that work, all spatial gradients vanished. There was no excitation whatsoever of hydrodynamic degrees of freedom, and the system relaxed exponentially toward equilibrium. In contrast, the dynamics of the boost-invariant plasma in the present work involves both hydrodynamic and nonhydrodynamic degrees of freedom. The results we present display a rather clear separation between far-from-equilibrium response, which cannot be described by hydrodynamics, followed by later ''near-local-equilibrium'' dynamics which is accurately described by viscous hydrodynamics. A noteworthy finding is that the domain of utility of hydrodynamics is not limited by when higher order terms in the hydrodynamic expansion become comparable to the lowest order viscous terms, rather it is determined by the relative importance of nonhydrodynamic degrees of freedom.

II. GRAVITATIONAL DESCRIPTION

Gauge/gravity duality [10] provides a gravitational description of large N_c SYM in which the 5D dual geometry is governed by Einstein's equations with a cosmological constant. Einstein's equations imply that the boundary metric $g^{\rm B}_{\mu\nu}(x)$, which characterizes the geometry of the spacetime boundary, is dynamically unconstrained. The specification of $g^{\rm B}_{\mu\nu}(x)$ serves as a boundary condition for the 5D Einstein equations. This reflects the fact that 4D gravitational dynamics is neglected; the dual field theory residing on the boundary responds to the boundary geometry but does not backreact on the 4D boundary geometry.

Diffeomorphism and spatial 3D translation invariance, together with our assumed $O(2)$ rotation invariance, allows one to chose a 5D bulk metric of the form

$$ds^2 = -Ad\tau^2 + \Sigma^2[e^B d\boldsymbol{x}_\perp^2 + e^{-2B}dy^2] + 2drd\tau, \quad (3)$$

where A, B, and Σ are all functions of the bulk radial coordinate r and time τ only. The coordinates τ and r are generalized infalling Eddington-Finkelstein coordinates. Infalling radial null geodesics have constant values of τ (as well as $\boldsymbol{x}_\perp$ and y). Outgoing radial null geodesics satisfy $dr/d\tau = \frac{1}{2}A$. The geometry in the bulk at $\tau > 0$ corresponds to the causal future of $\tau = 0$ on the boundary. The form of the metric (3) is invariant under the residual diffeomorphism $r \to r + f(\tau)$, where $f(\tau)$ is an arbitrary function.

With a metric of the form (3), Einstein's equations may be written very compactly as

$$0 = \Sigma(\dot{\Sigma})' + 2\Sigma'\dot{\Sigma} - 2\Sigma^2, \quad (4a)$$

$$0 = \Sigma(\dot{B})' + \tfrac{3}{2}(\Sigma'\dot{B} + B'\dot{\Sigma}), \quad (4b)$$

$$0 = A'' + 3B'\dot{B} - 12\Sigma'\dot{\Sigma}/\Sigma^2 + 4, \quad (4c)$$

$$0 = \ddot{\Sigma} + \tfrac{1}{2}(\dot{B}^2\Sigma - A'\dot{\Sigma}), \quad (4d)$$

$$0 = \Sigma'' + \tfrac{1}{2}B'^2\Sigma, \quad (4e)$$

where, for any function $h(r, \tau)$,

$$h' \equiv \partial_r h, \qquad \dot{h} \equiv \partial_\tau h + \tfrac{1}{2}A\partial_r h. \quad (5)$$

The derivative h' is a directional derivative of h along infalling radial null geodesics, while the derivative $\dot{h}$ is the directional derivative of h along outgoing null radial geodesics. Equations (4d) and (4e) are constraint equations; the radial derivative of Eq. (4d) and the time derivative of Eq. (4e) are implied by Eqs. (4a)–(4c).

The above set of differential equations must be solved subject to boundary conditions imposed at $r = \infty$. The requisite condition is simply that the boundary metric $g^{\rm B}_{\mu\nu}(x)$ coincide with our choice (1) of the 4D geometry.

In particular, we must have

$$\lim_{r\to\infty}\Sigma(r,\tau)/r \equiv \tau^{1/3}, \tag{6a}$$

$$\lim_{r\to\infty}B(r,\tau) \equiv -\tfrac{2}{3}\ln\tau + \gamma(\tau). \tag{6b}$$

One may fix the residual diffeomorphism invariance by also demanding that

$$\lim_{r\to\infty}[A(r,\tau) - r^2]/r = 0. \tag{7}$$

These boundary conditions, plus initial data satisfying the constraint (4e) on some $\tau = \tau_i$ slice, uniquely specify the subsequent evolution of the geometry.

Near the boundary one may solve Einstein's equations with a power series expansion in r. Specifically, A, B, and Σ have asymptotic expansions of the form

$$A(r,\tau) = \sum_{n=0}[a_n(\tau) + \alpha_n(\tau)\log r]r^{2-n}, \tag{8a}$$

$$B(r,\tau) = \sum_{n=0}[b_n(\tau) + \beta_n(\tau)\log r]r^{-n}, \tag{8b}$$

$$\Sigma(r,\tau) = \sum_{n=0}[s_n(\tau) + \sigma_n(\tau)\log r]r^{1-n}. \tag{8c}$$

The boundary conditions (6) and (7) imply that $b_0(\tau) \equiv -\frac{2}{3}\ln\tau + \gamma(\tau)$, $s_0(\tau) \equiv \tau^{1/3}$, $a_0(\tau) \equiv 1$, $a_1(\tau) \equiv 0$, and that the coefficients of the corresponding logarithmic terms vanish. Substituting the above expansions into Einstein's equations and solving the resulting equations order by order in r, one finds that there is one undetermined coefficient, $b_4(\tau)$. All other coefficients are determined by the boundary geometry, Einstein's equations, and $b_4(\tau)$.[2]

Given a solution to Einstein's equations, the SYM stress tensor is determined by the near-boundary behavior of the 5D metric [28]. If S_G denotes the gravitational action, then the SYM stress tensor is given by

$$T^{\mu\nu}(x) = \frac{2}{\sqrt{-g^B(x)}}\frac{\delta S_G}{\delta g^B_{\mu\nu}(x)}. \tag{9}$$

By substituting the above series expansions into the variation of the on-shell gravitational action, one may compute the expectation value of the stress tensor in terms of the expansion coefficients. This procedure has been carried out in Ref. [28], so we simply quote the results. In terms of the expansion coefficients, the SYM stress tensor reads

$$T^{\mu}{}_{\nu} = \frac{N_c^2}{2\pi^2}\,\mathrm{diag}(-\mathcal{E}, \mathcal{P}_\perp, \mathcal{P}_\perp, \mathcal{P}_\parallel), \tag{10}$$

where

$$\mathcal{E} = -\tfrac{3}{4}a_4 + \tilde{\mathcal{E}}, \tag{11a}$$

$$\mathcal{P}_\perp = -\tfrac{1}{4}a_4 + b_4 + \tilde{\mathcal{P}}_\perp, \tag{11b}$$

$$\mathcal{P}_\parallel = -\tfrac{1}{4}a_4 - 2b_4 + \tilde{\mathcal{P}}_\parallel, \tag{11c}$$

and

$$\tilde{\mathcal{E}} \equiv -\tfrac{5}{288}\gamma_1\tau^{-3} + \tfrac{5}{1152}(21\gamma_1^2 + 4\gamma_2)\tau^{-2} - \tfrac{1}{96}(3\gamma_1^3 - 8\gamma_1\gamma_2 - \gamma_3)\tau^{-1} + \tfrac{1}{256}(3\gamma_1^4 + 14\gamma_2^2 - 4\gamma_1\gamma_3), \tag{12a}$$

$$\tilde{\mathcal{P}}_\perp \equiv -\tfrac{1}{6}\tau^{-4} + \tfrac{227}{288}\gamma_1\tau^{-3} - \tfrac{1}{3456}(2397\gamma_1^2 + 1444\gamma_2)\tau^{-2} + \tfrac{1}{576}(57\gamma_1^3 + 488\gamma_1\gamma_2 + 70\gamma_3)\tau^{-1} + \tfrac{1}{768}(21\gamma_1^4 - 468\gamma_1^2\gamma_2 + 10\gamma_2^2 + 4\gamma_1\gamma_3 + 64\gamma_4), \tag{12b}$$

$$\tilde{\mathcal{P}}_\parallel \equiv \tfrac{1}{3}\tau^{-4} - \tfrac{449}{288}\gamma_1\tau^{-3} + \tfrac{1}{3456}(5379\gamma_1^2 + 2828\gamma_2)\tau^{-2} - \tfrac{1}{288}(120\gamma_1^3 + 458\gamma_1\gamma_2 + 73\gamma_3)\tau^{-1} + \tfrac{1}{768}(21\gamma_1^4 + 936\gamma_1^2\gamma_2 + 10\gamma_2^2 + 4\gamma_1\gamma_3 - 128\gamma_4), \tag{12c}$$

with $\gamma_n \equiv d^n\gamma/d\tau^n$.

III. NUMERICS

One may solve the Einstein equations (4a)–(4c) for the time derivatives $\dot{\Sigma}$, $\dot{B}$, and A''. Define

$$\Theta(r,\tau) \equiv \int_r^\infty dw[\Sigma(w,\tau)^3 - h_1(w,\tau)] - H_1(r,\tau), \tag{13a}$$

$$\Phi(r,\tau) \equiv \int_r^\infty dw[2\Theta(w,\tau)B'(w,\tau)\Sigma(w,\tau)^{-3/2} - h_2(w,\tau)] - H_2(r,\tau), \tag{13b}$$

where H_n is an indefinite radial integral of h_n,

$$h_n = H_n'. \tag{14}$$

Then Eqs. (4a)–(4c) are solved by

$$\dot{\Sigma} = -2\Theta\Sigma^{-2}, \tag{15a}$$

$$\dot{B} = -\tfrac{3}{2}\Phi\Sigma^{-3/2}, \tag{15b}$$

$$A'' = -4 - 24\Theta\Sigma'\Sigma^{-4} + \tfrac{9}{2}\Phi B'\Sigma^{-3/2}. \tag{15c}$$

The functions $h_n(r,\tau)$ are not constrained by Einstein's equations—their presence inside the integrands of Eq. (13) are compensated by the subtraction of their integrals $H_n(r,\tau)$. However, since we have chosen the upper limit of integration in Eq. (13) to be $r = \infty$, the functions $h_n(r,\tau)$ must be suitably chosen so that the integrals (13) are convergent. The simplest choice to accomplish this is to set $h_1(r,\tau)$ equal to the asymptotic expansion of $\Sigma(r,\tau)^3$

[2]The coefficient a_4 is determined by a first order ordinary differential equation, which can be obtained from the condition that the SYM stress tensor be covariantly conserved. All other coefficients are determined algebraically from $b_0(\tau)$, $b_4(\tau)$, $a_4(\tau)$, and their derivatives.

up to order $1/r^k$, for some $k > 1$, and to set $h_2(r, \tau)$ equal to the asymptotic expansion of $2\Theta(r, \tau)B'(r, \tau)/\Sigma(r, \tau)^{3/2}$ up to order $1/r^k$. In our numerical solutions reported below, we use $k \geq 4$. This choice makes the large r contribution to the integrals in Eq. (13) quite small and consequently reduces cutoff dependence. As the coefficients of the series expansions (8) only depend on $b_0(\tau)$ and $b_4(\tau)$ and their τ derivatives, this choice determines $h_n(r, \tau)$ in terms of one unknown function $b_4(\tau)$.

With the subtraction functions h_n specified by the aforementioned asymptotic expansions, integrating Eq. (14) fixes the compensating integrals H_n up to an integration constant which is an arbitrary function of τ. Integrating Eq. (15c) for $A(r, \tau)$ introduces two further (τ dependent) constants of integration. The most direct route for fixing these constants of integration is to match the large r behavior of the expressions (15a) and (15b) and the integrated version of Eq. (15c) to the corresponding expressions obtained from the series expansions (8). This fixes all integration constants in terms of b_0 and b_4.

Our algorithm for solving the initial value problem with time-dependent boundary conditions is as follows. At time τ_i the geometry is AdS_5 with the metric

$$ds^2 = r^2\left[-d\tau^2 + d\boldsymbol{x}_\perp^2 + \left(\tau + \frac{1}{r}\right)^2 dy^2\right] + 2dr d\tau. \quad (16)$$

Therefore, at the initial time τ_i we have

$$B(r, \tau_i) = -\frac{2}{3}\ln\left(\tau_i + \frac{1}{r}\right), \quad (17a)$$

$$\Sigma(r, \tau_i) = r\left(\tau_i + \frac{1}{r}\right)^{1/3}, \quad (17b)$$

$$A(r, \tau_i) = r^2. \quad (17c)$$

With $A(r, \tau_i)$, $B(r, \tau_i)$, and $\Sigma(r, \tau_i)$ known, one can then compute the time derivatives $\partial_\tau B(r, \tau_i)$ and $\partial_\tau \Sigma(r, \tau_i)$ from Eqs. (15b) and (15a), and step forward in time,

$$B(r, \tau_i + \Delta\tau) \approx B(r, \tau_i) + \partial_\tau B(r, \tau_i)\Delta\tau, \quad (18)$$

$$\Sigma(r, \tau_i + \Delta\tau) \approx \Sigma(r, \tau_i) + \partial_\tau \Sigma(r, \tau_i)\Delta\tau. \quad (19)$$

With $B(r, \tau_i + \Delta\tau)$ and $\Sigma(r, \tau_i + \Delta\tau)$ known, one can then integrate Eq. (15c) to determine $A(r, \tau_i + \Delta\tau)$. With the complete geometry on the time slice $\tau = \tau_i + \Delta\tau$ determined, one may then repeat the entire process and take another step forward in time.[3]

An important practical matter is fixing the computation domain in r—how far into the bulk does one want to compute the geometry? If a horizon forms, then one may excise the geometry inside the horizon as this region is causally disconnected from the geometry outside the horizon. Furthermore, one must excise the geometry to avoid singularities behind horizons [29]. To perform the excision, one first identifies the location of an apparent horizon (an outermost marginally trapped surface) which, if it exists, must lie inside an event horizon [30]. We have chosen to make the incision slightly inside the location of the apparent horizon. For the metric (3), the location $r_h(\tau)$ of the apparent horizon is given by the outermost point where $\dot{\Sigma}(r_h(\tau), \tau) = 0$ or, from Eq. (15a), $\Theta(r_h(\tau), \tau) = 0$.

IV. RESULTS AND DISCUSSION

We first discuss our results from the 5D gravitational perspective and present data for $c = 1$. Results for other values of c are presented below, but the qualitative features of the results are independent of the value of c. Figure 2 shows a congruence of outgoing radial null geodesics for $c = 1$. The geodesics are obtained by integrating $dr/d\tau = \frac{1}{2}A(r, \tau)$. The colored surface in the plot displays the value of A/r^2. Excised from the plot is a region of the geometry behind the apparent horizon, whose location is shown by the magenta dotted line.

At times $\tau < \tau_i = 1/4$, the boundary geometry is static and $A/r^2 = 1$. The outgoing geodesic congruence at early times therefore satisfies

$$\tau + 2/r = \text{const}, \quad (20)$$

and hence appears as parallel straight lines on the left side

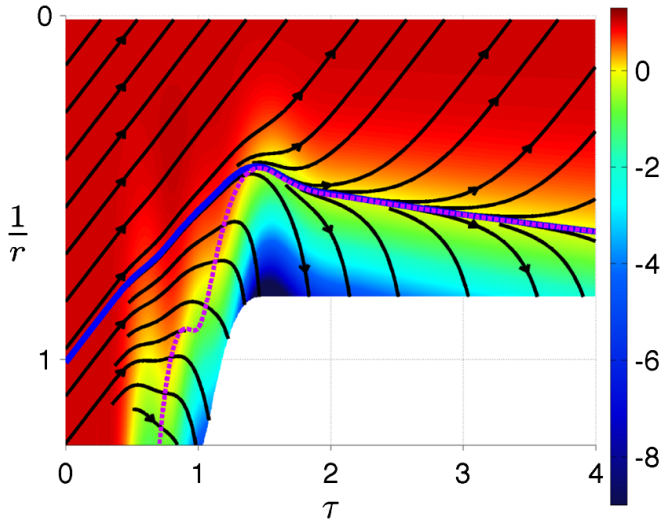

FIG. 2 (color online). The congruence of outgoing radial null geodesics. The surface coloring displays A/r^2. Before time $\tau_i = 1/4$ this quantity equals one. The excised region lies inside the apparent horizon, which is shown by the dashed magenta line. The geodesic shown as a solid blue line is the event horizon; it separates geodesics which escape to the boundary from those which cannot escape.

[3]Because we are working with a discretized version of Einstein's equations, the discretized version of the constraint equation (4a) is not automatically implied by the discretized version of the other Einstein equations. To minimize the amount of accumulated error, we also monitor the accuracy of the constraint equation (4a), and make tiny adjustments to Σ to prevent growing violation of the constraint.

of Fig. 2. These are just radial geodesics in AdS_5, which is the geometry dual to the initial zero temperature ground state. After time τ_i the boundary geometry starts to change, A/r^2 deviates from unity, and the congruence departs from the zero temperature form (20).

Perhaps the most dramatic feature in Fig. 2 is the formation of a bifurcation in the congruence of geodesics. As is evident from Fig. 2, at late times some geodesics escape up to the boundary and some plunge deep into the bulk. Separating escaping from plunging geodesics is precisely one geodesic that does neither. This geodesic, shown as the solid blue curve in the figure, defines the location of a null surface beyond which all events are causally disconnected from observers on the boundary. This surface is the event horizon of the geometry.

After the time $\tau_f = 2.25$, the boundary geometry becomes flat and unchanging, no additional gravitational radiation is produced, and the bulk geometry approaches a slowly evolving form. The rapid relaxation of high frequency modes can clearly be seen in the behavior of A/r^2 shown in Fig. 2—all of the high frequency structure in the plot appears only during the time interval where the boundary geometry is changing and creating gravitational radiation. Physically, the rapid relaxation of high frequency modes occurs because the horizon acts as an absorber of gravitational radiation and low frequency modes simply take more time to fall into the horizon than high frequency modes. Therefore, as time progresses the geometry relaxes onto a smooth universal form whose temporal variations become slower and slower as $\tau \to \infty$.

One can systematically construct late-time asymptotic expansions of boost-invariant solutions to Einstein's equations [7]. The expansion, which is a power series expansion in gradients, is dual to the hydrodynamic expansion in the field theory. This is natural, as the late-time evolution of the field theory state in conformal $\mathcal{N} = 4$ SYM must be described by hydrodynamics. In the gravitational setting, the metric is expanded in terms of 4D spacetime gradients of slowly varying fields. For the case of boost-invariant flow, each spacetime derivative introduces a factor of $1/(\Lambda\tau)^{2/3}$ into the solution, where Λ is an energy scale which characterizes the initial energy density [24]. The numerical coefficients of the expansion are related to transport coefficients in the dual gauge theory, and are independent of the initial conditions used to create the black hole geometry. Therefore, at asymptotically late times all sensitivity to the details of the initial conditions used to created the black hole geometry is isolated within the energy scale Λ, up to exponentially decreasing corrections to the late-time behavior.

At asymptotically late times, the boost-invariant gradient expansion of Ref. [24] yields a metric

$$ds^2 = r^2\left[-\left(1-\frac{r_h^4}{r^4}\right)d\tau^2 + d\boldsymbol{x}_\perp^2 + \tau^2 dy^2\right] + 2dr d\tau, \quad (21)$$

where $r_h(\tau) \approx \pi\Lambda/(\Lambda\tau)^{1/3}$ is the approximate location of the event and apparent horizons, whose positions asymptotically coincide at late times. The asymptotic metric (21) has a Hawking temperature

$$T_{\text{Hawking}} = \Lambda/(\Lambda\tau)^{1/3}, \quad (22)$$

which is proportional to the horizon radius $r_h(\tau)$. As time progresses, the horizon slowly falls deeper into the bulk, and the temperature of the black hole decreases as $\tau^{-1/3}$. The falling of the horizon into the bulk, as an inverse power of τ, is clearly visible in the numerical data presented in Fig. 2.

Figure 3 shows a plot of the area (per unit rapidity) of the event and apparent horizons, again for $c = 1$, as a function of τ. The area (per unit rapidity) of the apparent horizon is given by $\Sigma(r_h(\tau), \tau)^3$ where $r_h(\tau)$ is the apparent horizon location (given by a zero of $\dot{\Sigma}$). The area (per unit rapidity) of the event horizon is also given by Σ^3, but instead evaluated on the null geodesic defining the event horizon. The area of the apparent horizon starts off at zero, and grows rapidly for τ in the interval (τ_i, τ_f). This is to be expected, as it is during this interval of time that the rapid variation of the boundary geometry produces infalling gravitational radiation which is subsequently absorbed by the horizon. As radiation is absorbed, the horizon area must grow. After the production of radiation ceases, the geometry relaxes onto the asymptotic form (21) and the area (per unit rapidity) of the apparent and event horizons slowly approach a constant. From the figure, one sees that the growth of the apparent horizon area changes rather

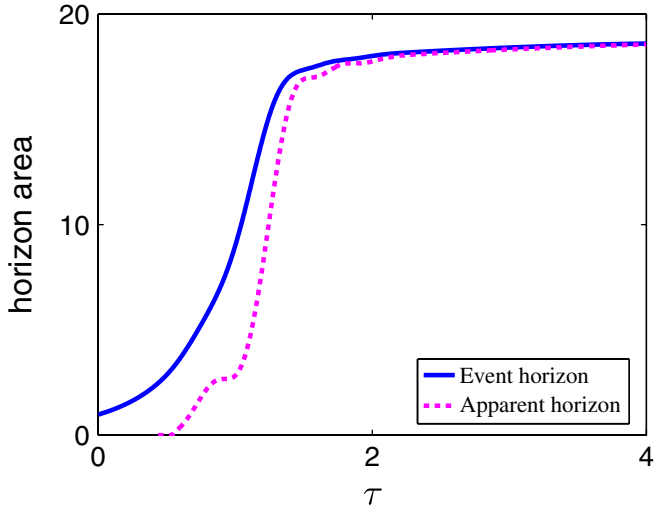

FIG. 3 (color online). Area of the event horizon and apparent horizon, per unit rapidity, as a function of proper time τ. The growth of the apparent horizon area, shown by the magenta dotted line, is causally connected to the changing boundary geometry. In contrast, the growth of the event horizon area, shown as a solid blue line, is nonzero at arbitrarily early times, long before the boundary geometry has started to change.

abruptly near time τ_f. This reflects of the fact that the boundary geometry ceases to produce infalling radiation after time τ_f. The flux of radiation through the horizon decreases dramatically after τ_f and correspondingly, so does the growth of the apparent horizon area.

In contrast to the apparent horizon area, which is nonzero only in the causal future of the boundary time τ_i, the event horizon area is nonzero arbitrarily far in the past, long before the boundary geometry starts to change. This reflects the teleological nature of event horizons. The event horizon separates events which are causally disconnected from boundary observers. As Fig. 2 clearly shows, even before the boundary geometry has started to change there are events which are causally disconnected from the boundary. These events are, by definition, behind the event horizon. Simply put, the black hole exists before the boundary deformation has begun.

Because the radial geodesic defining the event horizon is moving outwards at the speed of light, before the boundary geometry starts to change the area of the event horizon grows like $4(k+\tau)/(k-\tau)^3$, where k is the value of $\tau + 2/r$ on the geodesic defining the event horizon. The appropriate value of the constant k can only be determined when the entire future of the geometry is known.[4] Because of its acausal nature, the area of the event horizon cannot correspond to the entropy of the system in a nonequilibrium setting. In contrast, it does appear sensible to regard the apparent horizon area as a measure of thermodynamic entropy in a nonequilibrium setting.

To facilitate a quantitative comparison between our numerical solutions to Einstein's equations and the late-time gradient expansion of Ref. [24], Fig. 4 shows a close-up view of the areas (per unit rapidity) of the event and apparent horizons (EH and AH, respectively), together with the corresponding late-time asymptotic expansions, computed through second order in gradients. These asymptotic results are [25,31–33]

$$A_{\rm EH} = \pi^3\Lambda^2\left[1 - \frac{1}{2\pi(\Lambda\tau)^{2/3}} + \frac{6+\pi+6\ln 2}{24\pi^2(\Lambda\tau)^{4/3}}\right], \quad (23a)$$

$$A_{\rm AH} = \pi^3\Lambda^2\left[1 - \frac{1}{2\pi(\Lambda\tau)^{2/3}} + \frac{2+\pi+\ln 2}{24\pi^2(\Lambda\tau)^{4/3}}\right], \quad (23b)$$

for the event and apparent horizon areas, respectively, up to $\mathcal{O}((\Lambda\tau)^{-2})$ corrections. From the figure one sees that the asymptotic expansions, shown in the figure as the dashed black lines, agree very well with the complete numerical results. In fact, at time τ_f when the boundary geometry becomes flat, the asymptotic forms agree with the full numerical results for both horizon areas to within 0.11%.

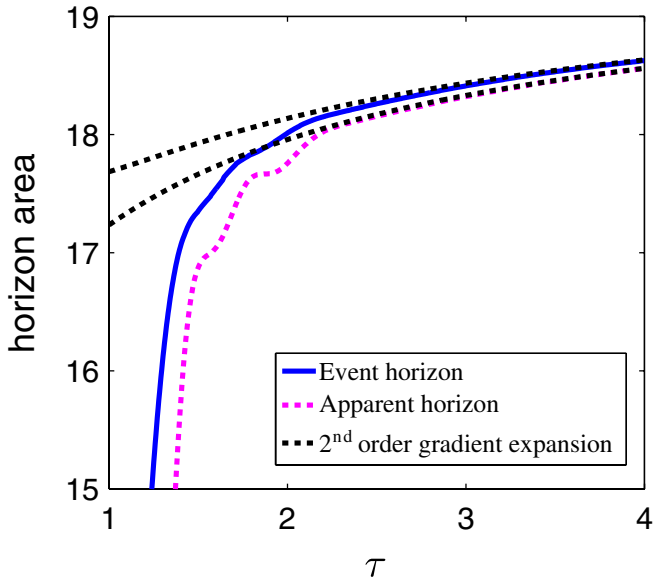

FIG. 4 (color online). Close-up view of the event horizon and apparent horizon areas, per unit rapidity, as a function of proper time τ, together with their corresponding asymptotic expressions (23). Both horizon areas are very well approximated by their asymptotic expansions, at second order in gradients, after time $\tau_f = 2.25$ when the boundary geometry becomes flat. Note the rather abrupt change in the growth of the apparent horizon area at τ_f.

For $c = 1$, our numerically measured value of Λ is 0.8. Consequently, the first order corrections appearing in Eqs. (23) generate 10% corrections at time τ_f, while the second-order terms yield 0.20% and 0.56% corrections to the event and apparent horizon areas, respectively.

This comparison shows that the geometry in the bulk (as probed by the horizon areas) is already very well approximated by the gradient expansion of Ref. [24] at time τ_f. However, it must be stressed that this very early agreement with hydrodynamics is specific to the horizon areas, and is not so true of other observables which are sensitive to the anisotropy in the geometry, such as the SYM stress tensor, which we discuss next.

We now turn to a discussion of our results for boundary field theory observables. Figure 5 shows plots of the energy density and transverse and longitudinal pressures produced by the changing boundary geometry (1), when $c = \pm 1$. These quantities begin at zero before time τ_i, when the system is in the vacuum state, and deviate from zero once the 4D geometry starts to vary. During the interval of time where the 4D geometry is changing, the energy density generally grows and the pressures rapidly oscillate: work is being done on the field theory state. After time τ_f the boundary geometry becomes flat and no longer does any work on the system. As time progresses, nonhydrodynamic

[4]This manifests itself as follows. At asymptotically late times, the location of the event horizon coincides with the zero of $A(r,\tau)$, so the unique outgoing radial geodesic that approaches the zero of $A(r,\tau)$ as $\tau \to \infty$ defines the event horizon. To locate the position of this geodesic at early times, and hence determine the horizon area, one must know the entire future of the geometry.

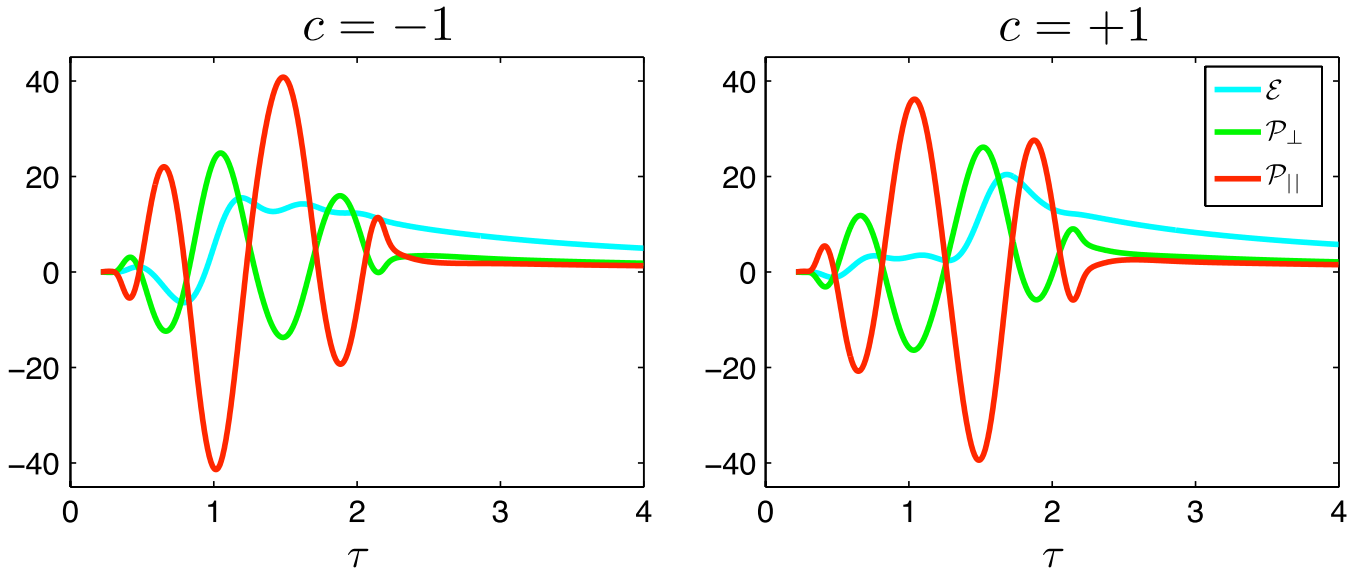

FIG. 5 (color online). Energy density, longitudinal and transverse pressure, all divided by $N_c^2/2\pi^2$, as a function of time for $c = -1$ (left) and $c = +1$ (right). The energy density and pressures start off at zero at time $\tau_i = 1/4$ when the system is in the vacuum state. During the interval of time $\tau \in (\tau_i, \tau_f) = (0.25, 2.25)$, the 4D geometry is changing and doing work on the field theory state. After time τ_f, the deformation in the geometry turns off and the field theory state subsequently relaxes onto a hydrodynamic description. The smooth tails in both plots occur during this regime. At late times, from top to bottom, the three curves (in both plots) correspond to the energy density $\mathcal{E}$, transverse pressure $\mathcal{P}_\perp$, and longitudinal pressure $\mathcal{P}_\parallel$.

degrees of freedom relax and at late times the evolution of the system is governed by hydrodynamics. The late-time hydrodynamic behavior manifests itself as the smooth tails appearing in Fig. 5.

The two sets of plots in Fig. 5, contrasting $c = +1$ and -1, are qualitatively similar, with the main difference being the phase of the oscillations in the pressures. For example, for $c = -1$ the transverse pressure is negative at τ_f whereas for $c = +1$ the transverse pressure is positive and larger than the longitudinal pressure, which is nearly zero at τ_f. As local equilibrium requires that the transverse and longitudinal pressure be nearly equal [3], one sees that in either case the system is far from equilibrium at τ_f. Furthermore, from the figure one sees that for either sign of c, the transverse pressure approaches the longitudinal pressure from above. As we discuss next, this is always the case in the hydrodynamic limit of boost-invariant flow.

From the gravitational asymptotic expansion of Ref. [24], one can compute the SYM stress tensor via Eq. (11). The results read [24]

$$\mathcal{E} = \frac{3\pi^4\Lambda^4}{4(\Lambda\tau)^{4/3}}\left[1 - \frac{2C_1}{(\Lambda\tau)^{2/3}} + \frac{C_2}{(\Lambda\tau)^{4/3}}\right], \tag{24a}$$

$$\mathcal{P}_\perp = \frac{\pi^4\Lambda^4}{4(\Lambda\tau)^{4/3}}\left[1 - \frac{C_2}{3(\Lambda\tau)^{4/3}}\right], \tag{24b}$$

$$\mathcal{P}_{||} = \frac{\pi^4\Lambda^4}{4(\Lambda\tau)^{4/3}}\left[1 - \frac{2C_1}{(\Lambda\tau)^{2/3}} + \frac{5C_2}{3(\Lambda\tau)^{4/3}}\right], \tag{24c}$$

up to $\mathcal{O}((\Lambda\tau)^{-2})$ corrections. The constant C_1 is related to the viscosity to entropy density ratio of the plasma, while the constant C_2 is related to second-order hydrodynamic relaxation times. For strongly-coupled SYM [25],

$$C_1 = \frac{1}{3\pi}, \qquad C_2 = \frac{2 + \ln 2}{18\pi^2}. \tag{25}$$

The form (24) for the stress energy can also be obtained from hydrodynamic considerations alone, together with knowledge of first- and second-order transport coefficients, and the assumption of boost invariance [34,35].

It is evident from the leading terms of the result (24) that at late times the stress-energy tensor approaches the ideal hydrodynamic form

$$T^\mu{}_\nu = \frac{\pi^2 N_c^2 T(\tau)^4}{8}\,\mathrm{diag}(-3, 1, 1, 1), \tag{26}$$

with a time-dependent temperature

$$T(\tau) = \Lambda/(\Lambda\tau)^{1/3}, \tag{27}$$

which matches the Hawking temperature (22) of the black brane in the gravitational description. The ideal stress tensor (26) is completely isotropic. Subleading terms in the result (24) show that the transverse pressure differs from the longitudinal pressure when viscous effects are taken into account. In particular, as mentioned above, first order viscous corrections make the transverse pressure larger than the longitudinal pressure.

To facilitate a quantitative comparison between our numerical results for the stress tensor and the late-time

hydrodynamic expansions, Fig. 6 shows the energy density and pressures for $c = 1/4$, 1, and $3/2$, with the corresponding hydrodynamic forms (24) plotted on top of the numerical data. The plots start at time $\tau = \tau_f$. In all three plots, one clearly sees the stress-energy components approach their hydrodynamic approximations. Moreover, in all plots one sees a substantial anisotropy even at late times where a hydrodynamic treatment is applicable. In other words, the effect of viscosity is very evident in these results.

Looking at Fig. 6, for time $\tau = \tau_f$ and $c = 1/4$, one sees that the transverse and longitudinal pressures are almost equal and opposite in magnitude at this time. So the system is initially very far from equilibrium. However, for $c = 3/2$ the pressures are both positive, and the system is much closer to equilibrium at τ_f. At first sight this might seem peculiar: how can it be that for larger values of c, where the size of the perturbation in the 4D geometry is huge, the system takes less time to reach local equilibrium. Qualitatively, this apparent puzzle is easy to understand. For large c, the changing geometry does more work on the system and consequently the system reaches a higher effective temperature. Because SYM is a conformal theory, relaxation times for nonhydrodynamic degrees of freedom must scale inversely with the temperature, and hence must vanish as the local energy density diverges. Therefore, in the $c \to \infty$ limit the system will always be very close to local equilibrium—even while the 4D geometry is changing—and the anisotropy in the pressures will vanish immediately at τ_f. As a consequence, one learns little about the physics of the relaxation of nonhydrodynamic degrees of freedom in the $c \to \infty$ limit.

Table I shows how various quantities characterizing the relaxation of the plasma depend on the boundary perturbation amplitude c, within the range $[-2, 2]$. Included in the table is the time τ_*, beyond which the stress tensor agrees with the hydrodynamic approximation (24) to within 10%. Also shown is the temperatures T_* at time τ_*, the scale Λ measured in units of τ_*, and the time intervals $\tau_* - \tau_i$ and $\tau_* - \tau_f$ measured in units of T_*.

From the table, one sees that as the magnitude of c increases, so does the temperature T_*. Moreover, as the magnitude of c increases, one sees that the time scale τ_* approaches $\tau_f = 2.25$. In particular, for $|c| = 2$ the stress tensor is already within 10% of its hydrodynamic limit at τ_f. As discussed above, both of these features are to be expected. Increasing $|c|$ means that the changing geometry does more work on the system, producing a larger energy density, and consequently the relaxation times of nonhydrodynamic degrees of freedom decrease. In all cases presented in Table I, the relevant dynamics—from the production of the plasma to its relaxation to near local equilibrium (where hydrodynamics applies)—occur over a time $\tau_* - \tau_i \lesssim 2/T_*$.

From Table I, one also sees that for $|c| \lesssim 1/2$ the time scale τ_* at which a hydrodynamic treatment becomes accurate occurs when $\Lambda\tau_* \approx 1$. For larger values of $|c|$, $\Lambda\tau_*$ is bigger. Examining the size of the coefficients in

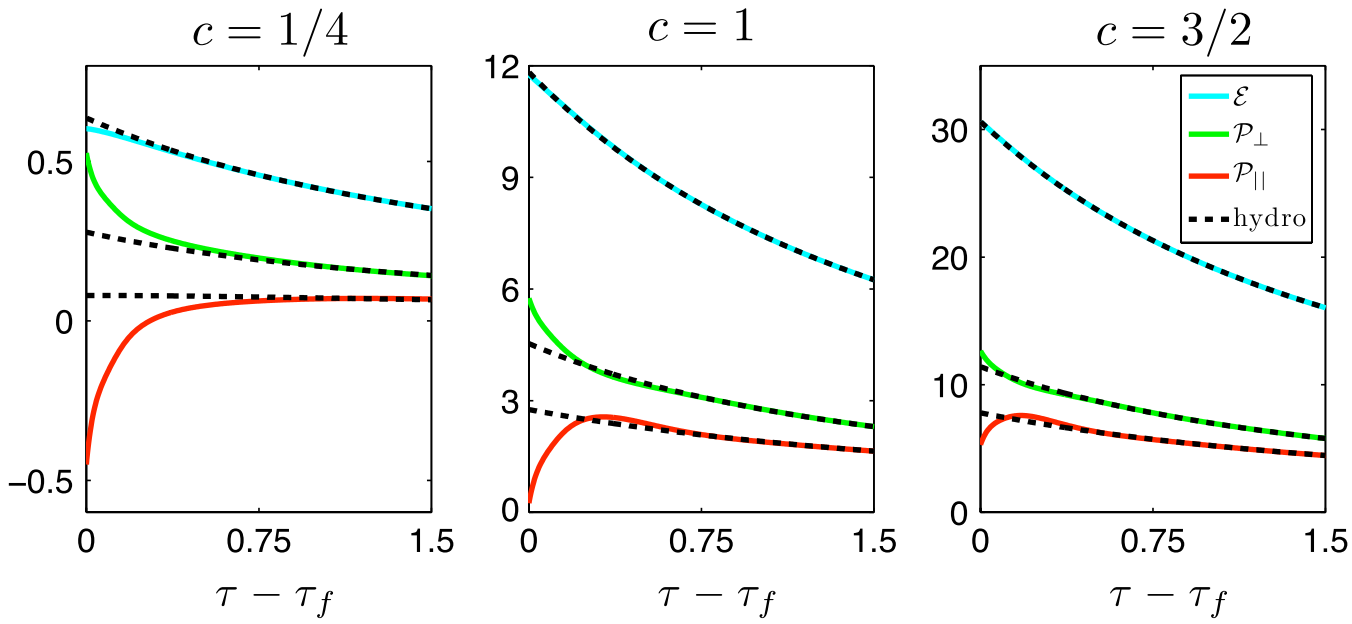

FIG. 6 (color online). Energy density, longitudinal and transverse pressure, all divided by $N_c^2/2\pi^2$, as a function of time for $c = 1/4$ (left), $c = 1$ (middle), and $c = 3/2$ (right). From top to bottom, the curves are energy density (blue), transverse pressure (green), and longitudinal pressure (red). The dashed black lines in each plot show the second-order viscous hydrodynamic approximation (24) to the different stress tensor components. Note the significantly different ordinate ranges in the three plots; the size of the difference between the transverse and longitudinal pressure grows with increasing c.

TABLE I. Quantities characterizing the relaxation to equilibrium, for various values of the boundary perturbation amplitude c. The relaxation time τ_* (in units of Δ) is the time at which the transverse and longitudinal pressures deviate from their hydrodynamic values (24) by less than 10%. T_* is the temperature at time τ_*, and Λ is the scale appearing in the hydrodynamic expansion (24) (both measured in units of Δ^{-1}). The quantity $(\tau_* - \tau_i)T_*$ measures the total time in units of T_* required to produce the plasma and relax to near local equilibrium. The quantity $(\tau_* - \tau_f)T_*$ measures the time in units of T_* required for the plasma to relax after the deformation in the geometry ceases. The quantity $[\mathcal{P}_\perp(\tau_f) - P_{||}(\tau_f)]/\mathcal{E}(\tau_f)$ is the pressure anisotropy, relative to the energy density, at time τ_f.

c	-2	$-3/2$	-1	$-1/2$	$-1/4$	$1/4$	$1/2$	1	$3/2$	2
τ_*	2.2	2.3	2.4	2.7	3.1	3.1	2.7	2.4	2.3	2.2
T_*	0.93	0.77	0.60	0.40	0.27	0.27	0.41	0.62	0.80	0.97
$\Lambda\tau_*$	3.1	2.5	1.9	1.2	0.87	0.89	1.3	1.9	2.6	3.3
$(\tau_* - \tau_i)T_*$	2.0	1.7	1.4	1.1	0.84	0.85	1.1	1.5	1.8	2.1
$(\tau_* - \tau_f)T_*$	0.00	0.05	0.11	0.19	0.24	0.24	0.20	0.11	0.04	0.00
$\frac{\mathcal{P}_\perp(\tau_f) - P_{\|\|}(\tau_f)}{\mathcal{E}(\tau_f)}$	0.06	-0.03	-0.22	-0.56	-1.1	1.6	0.91	0.47	0.24	0.13

Eq. (24) shows that the hydrodynamic expansion is quite well behaved for $\Lambda\tau \gtrsim 1$. From the time-temperature relation (27), one can convert $\Lambda\tau_* \gtrsim 1$ to the estimate $\tau_* T_* \gtrsim 1$ which, from Table I, is indeed the case.

Examining the size of the cofficients in the series (24) shows that the second-order $(\Lambda\tau)^{-4/3}$ terms are quite small compared to the leading $(\Lambda\tau)^{-2/3}$ viscous terms when $\Lambda\tau \geq 1$; they only become comparable when $\Lambda\tau$ is below 0.1. Hence, the fact that hydrodynamics is not accurate until $\Lambda\tau$ is larger than 1–2 (depending on the value of c) indicates that the physics which determines the onset of hydrodynamic behavior is not responsible for higher order terms in the hydrodynamic expansion becoming comparable to lower order terms. Rather, the change in behavior from nonhydrodynamic far-from-equilibrium behavior to near-local-equilibrium hydrodynamic response must be reflecting the relative importance of exponentially relaxing nonhydrodynamic degrees of freedom in comparison to the slowly relaxing hydrodynamic modes. This means that one cannot accurately identify the domain of utility of the hydrodynamic description by asking when the late-time gradient expansion breaks down. A similar conclusion was also reached in Ref. [36] by analyzing small perturbations on top of an infinite static plasma.

It is instructive to discuss the qualitative origin of the relaxation time τ_* from the perspective of the 5D gravitational problem. First consider the limit $|c| \to \infty$. In this limit, large amounts of gravitational radiation are produced by the changing boundary geometry and the amount of energy which falls deep into the bulk diverges. As a consequence, the horizon radius must approach the boundary as $|c| \to \infty$. The infall time for radiation to travel from the boundary to the horizon is roughly equal to the inverse horizon radius (in our coordinate system), so in the $|c| \to \infty$ limit, the geometry outside the horizon effectively responds instantaneously to the changing boundary geometry. Therefore, as $|c| \to \infty$, the system needs no to time to return to local equilibrium after the geometry stops changing at time τ_f.

Now consider the $|c| \to 0$ limit. For small $|c|$, distinct dynamics occurs on the time scales Δ and $\Delta/\sqrt{|c|}$ [with $\Delta \equiv \frac{1}{2}(\tau_f - \tau_i)$]. First of all, irrespective of how small c is, the positions of the apparent and event horizons are rapidly varying only over the time scale Δ. This is because it is during the time interval $\tau_i \leq \tau \leq \tau_f$ that gravitational radiation is being produced and absorbed by the horizon, creating most growth in horizon area. The parametric size of the horizon radii at τ_f is $\sim\sqrt{|c|}/\Delta$. Qualitatively, this makes sense since little radiation is produced and very little radiation falls into the bulk of the geometry when $|c|$ is small. Hence, the black hole size will vanish as $|c| \to 0$. An easy way to understand the $\sqrt{|c|}$ scaling is to note that the total energy added to the field theory state cannot depend on the sign of c, and therefore must be quadratic in c in the small $|c|$ limit. The final state energy density in the field theory will scale as r_h^4, so the horizon radii must be proportional to $\sqrt{|c|}$. Consequently, after time τ_f it takes a time $\sim\Delta/\sqrt{|c|}$ for any remaining short wavelength perturbations to fall into the horizon. It is during this interval of time that the geometry undergoes its relaxation onto the slowly evolving hydrodynamic form. We therefore see that $\tau_* T_*$ should have a nonzero $\mathcal{O}(1)$ limit when $|c| \to 0$.[5]

Last, we discuss the relevance of our work to more complicated numerical relativity problems in gauge/gravity duality. As discussed in the Introduction, an interesting future direction is the study of collisions of gravitational

[5]A brief comment on the relation between our work and the recent paper of Bhattacharyya and Minwalla [22] may be in order. These authors examined black hole formation and thermalization in response to an arbitrarily weak boundary perturbation coupling to the dilaton. A noteworthy finding in this work was "instant thermalization" (as probed by measurements of local operators) after the boundary perturbation turned off. However, this is the case for asymptotically AdS_4 spacetime and, as clearly stated in Ref. [22], is not expected to hold in asymptotically AdS_5 spacetime or for noninfinitesimal boundary perturbations.

shock waves in AdS_5, as this is dual to the collision of sheets of matter in SYM and mimics the collision of large, highly boosted nuclei in heavy-ion collisions. In the simplest setting, one can study shock waves which are translationally invariant in two transverse directions [16]. The corresponding gravitational problem is therefore $2+1$ dimensional. While we have studied a simpler $1+1$ dimensional gravitational problem in this paper, there are several lessons which may provide insight relevant for more difficult problems. First, we found it necessary to solve Einstein's equations analytically near the boundary with a power series expansion in the radial coordinate. This was required as the presence of the negative cosmological constant makes the near-boundary geometry singular. More specifically, careful asymptotic near-boundary analysis was required to determine the appropriate subtraction terms needed to make the integrals (13) finite and produce a numerical scheme which remains accurate near the boundary. The same issue will arise in gravitational problems with less symmetry.

Another important lesson concerns the choice of coordinates. Because of the presence of the negative cosmological constant, all matter and radiation tends to fall inward into the bulk. This universality of gravitational infall motivates the use of coordinates specifically adapted for infalling motion. The generalized infalling Eddington-Finkelstein coordinates we used, which assign a constant "time" coordinate to all events on infalling null radial geodesics, are especially appropriate for numerics. Had we used a time coordinate which defined a spacelike slicing of the geometry, then we would have wasted computational time solving for the geometry deep in the bulk before any signals from the boundary had arrived. With a null time coordinate, a signal propagating in from the boundary at $r=\infty$ arrives "*instantaneously*" at $r=0$. Moreover, the generalized infalling Eddington-Finkelstein coordinates yield a metric (3) which is nonsingular on the horizon. Coordinates which do not yield a metric regular at the horizon, such as Fefferman-Graham coordinates, are not well suited to numerical initial value problems.

V. CONCLUSIONS

Using gauge/gravity duality, we have studied the production and relaxation of a boost-invariant plasma in strongly-coupled $\mathcal{N}=4$ supersymmetric Yang-Mills theory. The production mechanism is a time-dependent deformation of the four-dimensional geometry in which the field theory lives. The deformation, which was confined to a compact interval of proper time, does work on the system and thus excites the initial state, which we took to the $\mathcal{N}=4$ SYM vacuum. Within the context of gauge/gravity duality, this problem maps into the problem of black hole formation in five dimensions. By solving the corresponding gravitational problem numerically, and using the gauge/gravity dictionary, we were able to compute the field theory stress tensor at all times, from the first excitation of the initial vacuum state to the late-time onset of hydrodynamics. We found that the entire process of plasma creation—from the initial vacuum state to the relaxation onto a hydrodynamic description—can occur in times as short as 1 to 2 times $1/T_*$, where T_* is the local temperature at the onset of the hydrodynamic regime. We also demonstrated that the time at which a hydrodynamic treatment first becomes valid does not coincide with the point where the hydrodynamic gradient expansion breaks down. This reflects the fact that in a far-from-equilibrium state there are nonhydrodynamic degrees of freedom. These modes relax exponentially, and their relative importance determines the onset of the hydrodynamic regime.

This work, together with our earlier paper [21], provide novel additions to the very sparse set of examples of genuinely far-from-equilibrium processes in quantum field theory which can be studied with complete theoretical control. Using techniques similar to those presented in this paper, it should be possible to study more demanding problems which have less symmetry.

ACKNOWLEDGMENTS

This work was supported in part by the U.S. Department of Energy under Grant No. DE-FG02-96ER40956. We are grateful to Michal Heller, Andreas Karch, and Paul Romatschke for useful discussions.

[1] P. Arnold, G. D. Moore, and L. G. Yaffe, J. High Energy Phys. 01 (2003) 030.
[2] P. Arnold, G. D. Moore, and L. G. Yaffe, J. High Energy Phys. 05 (2003) 051.
[3] P. Arnold, J. Lenaghan, G. D. Moore, and L. G. Yaffe, Phys. Rev. Lett. **94**, 072302 (2005).
[4] P. Arnold, G. D. Moore, and L. G. Yaffe, J. High Energy Phys. 11 (2000) 001.
[5] S. Jeon and L. G. Yaffe, Phys. Rev. D **53**, 5799 (1996).
[6] P. Kovtun, D. T. Son, and A. O. Starinets, Phys. Rev. Lett. **94**, 111601 (2005).
[7] S. Bhattacharyya, V. E. Hubeny, S. Minwalla, and M. Rangamani, J. High Energy Phys. 02 (2008) 045.
[8] P. M. Chesler and L. G. Yaffe, Phys. Rev. D **78**, 045013 (2008).
[9] P. K. Kovtun and A. O. Starinets, Phys. Rev. D **72**, 086009 (2005).
[10] J. M. Maldacena, Adv. Theor. Math. Phys. **2**, 231 (1998).

[11] E. Witten, Adv. Theor. Math. Phys. **2**, 253 (1998).
[12] S. S. Gubser, I. R. Klebanov, and A. M. Polyakov, Phys. Lett. B **428**, 105 (1998).
[13] E. Shuryak, Prog. Part. Nucl. Phys. **53**, 273 (2004).
[14] E. V. Shuryak, Nucl. Phys. **A750**, 64 (2005).
[15] U. W. Heinz, AIP Conf. Proc. **739**, 163 (2004).
[16] D. Grumiller and P. Romatschke, J. High Energy Phys. 08 (2008) 027.
[17] S. S. Gubser, S. S. Pufu, and A. Yarom, Phys. Rev. D **78**, 066014 (2008).
[18] L. Alvarez-Gaume, C. Gomez, A. S. Vera, A. Tavanfar, and M. A. Vazquez-Mozo, J. High Energy Phys. 02 (2009) 009.
[19] S. Lin and E. Shuryak, Phys. Rev. D **79**, 124015 (2009).
[20] S. S. Gubser, S. S. Pufu, and A. Yarom, J. High Energy Phys. 11 (2009) 050.
[21] P. M. Chesler and L. G. Yaffe, Phys. Rev. Lett. **102**, 211601 (2009).
[22] S. Bhattacharyya and S. Minwalla, J. High Energy Phys. 09 (2009) 034.
[23] N. D. Birrell and P. C. W. Davies, *Quantum Fields in Curved Space* (Cambridge University Press, England, 1982).
[24] R. A. Janik and R. B. Peschanski, Phys. Rev. D **73**, 045013 (2006).
[25] S. Kinoshita, S. Mukohyama, S. Nakamura, and K.-y. Oda, Prog. Theor. Phys. **121**, 121 (2009).
[26] M. P. Heller, P. Surowka, R. Loganayagam, M. Spalinski, and S. E. Vazquez, Phys. Rev. Lett. **102**, 041601 (2009).
[27] G. Beuf, M. P. Heller, R. A. Janik, and R. Peschanski, J. High Energy Phys. 10 (2009) 043.
[28] S. de Haro, S. N. Solodukhin, and K. Skenderis, Commun. Math. Phys. **217**, 595 (2001).
[29] P. Anninos, G. Daues, J. Masso, E. Seidel, and W.-M. Suen, Phys. Rev. D **51**, 5562 (1995).
[30] R. M. Wald, *General Relativity* (Chicago University Press, Chicago, 1984), p. 491.
[31] S. Nakamura and S.-J. Sin, J. High Energy Phys. 09 (2006) 020.
[32] P. Figueras, V. E. Hubeny, M. Rangamani, and S. F. Ross, J. High Energy Phys. 04 (2009) 137.
[33] I. Booth, M. P. Heller, and M. Spalinski, "Gravity Dual to Boost-Invariant Flow as a Slowly-Evolving Geometry" (unpublished).
[34] J. D. Bjorken, Phys. Rev. D **27**, 140 (1983).
[35] R. Baier, P. Romatschke, D. T. Son, A. O. Starinets, and M. A. Stephanov, J. High Energy Phys. 04 (2008) 100.
[36] I. Amado, C. Hoyos-Badajoz, K. Landsteiner, and S. Montero, J. High Energy Phys. 07 (2008) 133.